Vol. 22, No. 3(2023) Proc2884
Revista Mexicana de Ingeniería Química

Determination of interfacial energy of the system acetylsalicylic acid-ethanol using the 3D nucleation theory and the integral method

Determinación de la energía interfacial del sistema ácido acetil salicílico-etanol aplicando la teoría de nucleación 3D y el método integral

X.M. Medina-Galvan*, P. A. Quintana-Hernández, E. M. Escamilla-Silva, L. F. Fuentes-Cortés

Departamento de Ingeniería Química. Tecnológico Nacional de México en Celaya. ITC. Antonio García Cubas Pte. # 600 esq. Av. Tecnológico, Celaya, Guanajuato, 38010, México.

Received: July 13, 2021; Accepted: December 14, 2022

Abstract

In this work, the interfacial energy of the acetylsalicylic acid-ethanol system was evaluated using experimental results of the metastable zone width (MSZW) obtained at the following operation conditions: agitation rate (230 and 400 rpm), cooing rate (6, 9, 12 and 15 K/h) and saturation temperature (288.15, 293.15, 298.15, 303.15, 308.15 and 313.15 K). A nonlinear regression algorithm and an easy to implement a lineal integration algorithm of the number density of nuclei were used to determine the interfacial energy. The results obtained with the two integral strategies were compared with the values obtained with the 3D nucleation theory. Interfacial energies obtained with the nonlinear regression presented a difference smaller than 6.5 % but estimations determined with the lineal integration algorithm had an average difference of 48.6 %.

Keywords: acetylsalicylic acid, anhydrous ethanol, crystallization, integral method, interfacial energy.

Resumen

En este trabajo se determinaron los valores de la energía interfacial del sistema ácido acetil salicílico-etanol a partir de datos experimentales del ancho de la zona metaestable (AZM) obtenidos a las siguientes condiciones de operación: velocidad de agitación (230 y 400 rpm), velocidad de enfriamiento (6, 9, 12 y 15 K/h) y temperatura de saturación (288.15, 293.15, 298.15, 303.15, 308.15 y 313.15 K). Un algoritmo de regresión no lineal y otro de integración lineal fácil de desarrollar fueron usados para determinar la energía interfacial. Los resultados obtenidos por medio de los métodos integrales fueron comparados con los obtenidos por medio de la teoría de nucleación 3D. Las energías interfaciales estimadas con la regresión no lineal presentaron una diferencia menor a 6.5 %, mientras que las estimaciones determinadas con el algoritmo de integración lineal tuvieron una diferencia promedio del 48.6%.

Palabras clave: ácido acetil salicílico, etanol anhidro, cristalización, método integral, energía interfacial.

*Corresponding author. *E-mail*: xochitl.medina@iqcelaya.itc.mx
https://doi.org/10.24275/rmiq/Proc2884
ISSN:1665-2738, *issn-e*: 2395-8472

1 Introduction

Acetylsalicylic acid (ASA) has been recognized for its great medical importance, as an active ingredient of aspirin. It has been used as an analgesic, antipyretic and platelet antiaggregant. The ASA is produced by a chemical reaction of salicylic acid with acetic anhydride in the liquid phase; later, it is purified through crystallization stages that allow reaching high purities.

On the other hand, crystallization has been analyzed using distributed parameters models that include population, mass and energy balances coupled with the two transfer mechanisms equations that describe the phenomena of nucleation and growth. Nucleation is dominant when the solution is highly supersaturated and growth is controlled keeping supersaturation within the metastable zone width (MSZW). Determination of the MSZW is usually experimentally performed as function of some operation conditions, such as, cooling rate, saturation temperature, agitation rates, etc. In addition, MSZW data have been used to evaluate kinetic and thermodynamic parameters used for developing robust strategies for the crystallization process control. Up to date, no theoretical models have been developed for the evaluation of crystallization kinetic and thermodynamics parameters, so experimental determination is still frequent.

The interfacial energy is an important thermodynamic parameter related to the required energy for the mass transfer of the solute from the liquid phase to the solid phase. It has been usually associated to the formation of critical nuclei (thermodynamically stable) and represents the beginning of the nucleation process. Estimation of the interfacial energy has been performed by different strategies. Sangwal (2009) combined the experimental measurements of the MSZW and the 3D nucleation theory. He related the nucleation rate with the solution supersaturation, dissolution enthalpy and the number density of nuclei, which is difficult to evaluate. Shiau and Wu (2020) proposed two different strategies for evaluating the integral of the number density nuclei, to determine the pre-exponential factor and interfacial energy from MSZW data and cooling rate. Both algorithms are easy to implement and evaluate the integration of the number density of nuclei using a nonlinear and a linear adjustment regression obtaining the values for the interfacial energy in a more direct way.

Interfacial energies for the system ASA in ethanol have been reported for similar operation conditions by Medina, *et al*., (2022). The energies were determined with the 3D nucleation strategy. In this work, the much simple integral approaches are described and the results are compared to those obtained with the 3D nucleation approach, determining the difference that exists between the three methods used, analyzing if the integral and linearized integral methods are a good approximation for the calculation of the interfacial energy and the pre-exponential for the system acetylsalicylic acid in ethanol.

2 Theory

2.1 *Classical three-dimensional nucleation theory approach*

According to the classical 3D nucleation theory (Sangwal, 2009a,b) the nucleation rate J is related to supersaturation as follows:

$$J = A\exp\left[-\frac{B}{(\ln S)^2}\right] \tag{1}$$

where the parameter B is defined by Eq. (2) for spherical particles; A is the pre-exponential constant related to the kinetics of nuclei formation in the growth medium and S is the relative solubility.

$$B = \frac{16\pi}{3}\left(\frac{\gamma\Omega^{2/3}}{k_B T_{\max}}\right)^3 \tag{2}$$

The parameters γ and Ω represent the solid-liquid interfacial energy and the molecular volume of solute, respectively; k_B is the Boltzmann constant and $T_{\max}$ is the temperature at the MSZW limit. The relative solubility can be expressed in terms of the van't Hoff equation, Eq. (3), as function of concentrations or the dissolution heat.

$$\ln S = \ln\left(\frac{C_0}{C_{\max}}\right) = \frac{-\Delta H_d}{R_g}\left(\frac{1}{T_0} - \frac{1}{T_{\max}}\right) = \left(\frac{\Delta H_d}{R_g T_{\max}}\right)\left(\frac{\Delta T_{\max}}{T_0}\right) \tag{3}$$

The parameters C_0 corresponds to the concentration at the saturation temperature, T_0; $C_{\max}$ is the concentration at the MSZW limit; ΔH_d is the dissolution heat and R_g is the ideal gas constant. Sangwal (2009b) derived Eq. (4) relating the maximum supercooling, $\Delta T_{\max}$ of the MSZW, the

saturation temperature (T_0) and the cooling rate (R).

$$\left(\frac{T_0}{\Delta T_{\max}}\right)^2 = F - F_1 \ln R \tag{4}$$

A plot of $(T_0/\Delta T_{\max})^2$ versus $\ln R$ generates a straight line with slope F_1. This parameter is related to B as shown in Eq. (5).

$$F_1 = \frac{1}{B}\left(\frac{\Delta H_d}{R_g T_{\max}}\right)^2 \tag{5}$$

Combining eqs. (2) and (5) and solving for γ generate Eq. (6) for the interfacial energy.

$$\gamma = \left(\frac{3k_B^3 T_{\max}\Delta H_d^2}{16\pi F_1 R_g^2 \Omega^2}\right)^{1/3} \tag{6}$$

2.2 *Integral method*

Shiau and Wu (2020) derived another approach for estimating the interfacial energy. They evaluated the number density of nuclei as defined by Eq. (7) and assumed a constant cooling rate given by Eq. (8).

$$f_N = \int_0^{t_{\max}} J dt \tag{7}$$

$$R = -\frac{dT}{dt} \quad (R > 0) \tag{8}$$

Substituting eqs. (1-3) and (8) into Eq. (7) generates the ratio of the number density of nuclei and the pre exponential factor.

$$\frac{f_N}{A} = -\int_{T_0}^{T_{\max}} \exp\left[-\left(\frac{16\pi\Omega^2\gamma^3}{3k_B^3 T_{\max}}\right)\left(\frac{T_0 R_g}{\Delta H_d \Delta T_{\max}}\right)^2\right]\frac{dT}{R} \tag{9}$$

Eq. (9) was solved by a nonlinear regression algorithm following the next four steps: (a) guess γ; (b) determine $(A/f_N)_j$ integrating Eq. (9) for each pair of $T_{\max}$ vs R; (c) calculate the averaged value $(A/f_N)_{av}$ with Eq. (10); (d) calculate the coefficient of variation (CV) among all $(A/f_N)_j$ with Eq. (11). The lowest CV value produces the best estimation of γ and A/f_N.

$$\left(\frac{A}{f_N}\right)_{av} = \frac{1}{H}\sum_{j=1}^{H}\left(\frac{A}{f_N}\right)_j \tag{10}$$

where H is the number of experimental data points ($H \geq 2$). For the guessed γ, CV among all $(A/f_N)_j$ is defined as:

$$CV = -\frac{\sqrt{\frac{1}{H-1}\sum_{j=1}^{H}\left[\left(\frac{A}{f_N}\right)_j - \left(\frac{A}{f_N}\right)_{av}\right]^2}}{\left(\frac{A}{f_N}\right)_{av}} \tag{11}$$

2.3 *Linearized integral method*

A simplified version for integrating Eq. (7) was obtained using the trapezoidal rule.

$$f_N = \frac{\Delta T_{\max}}{2R}(J_0 + J_{\max}) \tag{12}$$

where J_0 and $J_{\max}$ represent the nucleation rate at T_0 and $T_{\max}$.

Substituting eqs. (1-3) into Eq. (12), taking logarithm on both sides and rearranging generate Eq. (13) for the linearized integral method evaluation.

$$\frac{1}{T_{\max}}\left(\frac{T_0}{\Delta T_{\max}}\right)^2 = \frac{3}{16\pi}\left(\frac{k_B^3}{\Omega^2\gamma^3}\right)\left(\frac{\Delta H_d}{R_g}\right)^2 \left[\ln\left(\frac{\Delta T_{\max}}{R}\right) + \ln\left(\frac{A}{2f_N}\right)\right] \tag{13}$$

A plot of $\frac{1}{T_{\max}}(T_0/\Delta T_{\max})^2$ versus $\ln(\Delta T_{\max}/R)$ at a given T_0 should give a straight line. The parameters γ and A/f_N are evaluated from the information provided by the slope and intercept without the knowledge of f_N.

3 Methods

3.1 *Materials*

The materials used for the experiments were acetylsalicylic acid (CAS No. 50-78-2) with mass purity of 99% w/w and anhydrous ethanol (CAS No. 64-17-5) with purity of 99%, both Golden Bell brand.

3.2 *Equipment*

The experimental equipment used for this work is shown in Figure 1. It consists of a stainless-steel crystallizer of three-liter capacity Pignat (Pilot Unit No. 9312122, Pignat, France), The system is cooled with a LAUDA RP1800 thermal bath (Lauda-Konigshofen, Germany). The agitation rate is controlled with an agitator RW20DZM, Jake & Kunkel (USA).

The particle size was measured with a Mastersizer S (Marven Instruments Ltd. England) with a detection range between 0.5-880 μm. The solution temperature were measured with a cDAQ9401 (National Instruments, USA).

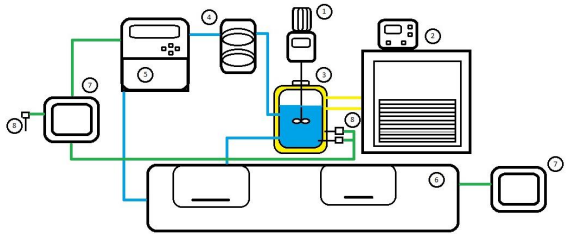

Figure 1. Diagram of the equipment used in the experimentation, 1) agitator, 2) thermal bath, 3) crystallizer. 4) peristatic pump, 5) Densitometer, 6) Master Sizer, 7) computer equipment and 8) thermocouple.

3.3 Metastable zone width experiments

The saturated solutions were prepared with 1500 cm^3 of ethanol and the corresponding mass of ASA [Maia and Giulietti 2008; Medina 2018 and Medina *et al*. 2020] for every saturation temperature (288.15, 293.15, 298.151, 303.15, 308.15 and 313.15 K), Solutions were heated 10 K above their saturation temperature for 30 minutes ensuring their complete dissolution. Each sample was cooled following the proposed lineal profiles (6, 9, 12 and 15 K/h). For reproducible mixing conditions, the agitation rates were kept constant at the specified values during the experiments using two agitation rates (230 and 400 rpm). The MSZW was determined when stable crystals appeared on the Master Sizer measurements with a minimum detection size of 1μm. Experiments were performed by triplicate at every experimental condition. Temperature and crystal size distributions were measured on line every 30 seconds.

4 Results and discussion

4.1 Evaluation of the metastable zone width

Figure 2 shows the profiles of the MSZW at different operating conditions. MSZW gets wider as cooling rates, agitation rates and saturation temperatures increase. High cooling rates produce temperature profiles that change rapidly over time and it is difficult that the solution temperature follow those profiles. The record of temperature at which new nuclei appear presents a delay that makes the MSZW wider.

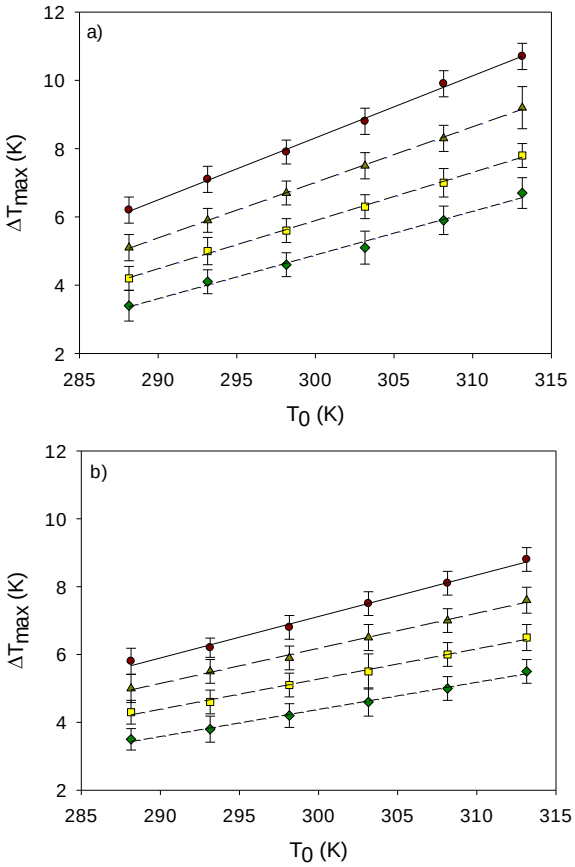

Figure 2. Plots MSZW vs T_0 at different cooling rates profiles: ● 15 K h^{-1}, ▲ 12 K h^{-1}, ■ 9 K h^{-1} and ♦ 6 K h^{-1} and different agitation rate: a) 400 rpm and b) 230 rpm.

On the other hand, the MSZW usually decreases when agitation rates increase. High agitation rates are usually associated with better mass transfer, since the probability of effective collisions between molecules increases the birth of new nuclei. However, some authors have reported the existence of a limit for the agitation speed. When agitation rates are above the limit, the mass transfer does not improve because of the presence of other mixing effects. Mohd-Noor *et al*. (2020) described the presence of a critical agitation rate in the range of 350-400 rpm. Above the limit, the common behavior reversed for some systems such as: p-aminobenzoic acid and ammonium dihydrogen phosphate in aqueous solutions. Chianese and Kramer (2012) reported a reversed behavior for other systems at high agitation rates and concluded that the overall effect of agitation on the MSZW was highly influenced by the solute and solvent thermodynamic properties.

On the other hand, it is common that the MSZW

decreases as the saturation temperature increases. However, in this study, the opposite behavior was shown. In the literature, only a few systems have shown this opposite behavior (Hansen *et al*., 2016; Mielniczek, 2014; Muñoz, 2020; Sun *et al*., 2005; Xiong *et al*., 2018 and Zhang *et al*., 2015). This less common behavior has been related to the formation of large clusters of molecules that enhance both the interactions among the molecules and the activation energy. These two actions delay the birth of new nuclei.

4.2 Interfacial energy

Table 1 shows the results of the fit of Eq. (4) for the 3D nucleation approach at the two agitation rates. Figure 3 shows the experimental data and adjusted models with the linearized integral method.

Table 2 shows the estimated values for the interfacial energy calculated with the 3D nucleation approach (average values over the different cooling rates), Eq. (6); the nonlinear integral method, Eq. (9); and the linearized integral method, Eq. (13) at different saturation temperatures. The birth of new nuclei results easier when the required interfacial energy is low. For the system ASA-ethanol, an increment in saturation temperature requires an increment in the necessary energy for the formation of new nuclei. As mentioned before, this is the result of the highly stable cluster of dissolved molecules (Shiau 2021; Shiau and Wu 2020 and Shiau 2018). On the other hand, an increment in the agitation rate reduces the required interfacial energy only at a very low saturation temperature. For highly concentrated solutions, more energy is required when agitation is high. This behavior suggested that large agitation rates improved convective mass transfer only at low saturated solutions.

The interfacial energy values obtained with the integral methods were larger than those values determined with the 3D nucleation theory at 230 rpm. The linear approach produced larger interfacial energies that the nonlinear approach. A comparison of the nonlinear and linear integral approaches to the 3D nucleation approach showed a relative difference of 6.47% and 48.6 %. The trapezoidal rule used in the linear integral approach generated a large difference. It seemed that the linear approach was not suitable for the evaluation of the interfacial energy for the system ASA-ethanol.

Table 1. Estimated kinetic parameters values using the 3D nucleation theory approach.

T_0 (K)	230 rpm			400 rpm		
	$F \times 10^{-4}$	$F_1 \times 10^{-3}$	R^2	$F \times 10^{-4}$	$F_1 \times 10^{-3}$	R^2
288.15	1.5061	4.7032	0.9905	1.6948	5.5055	0.9964
293.15	1.3240	4.1246	0.9909	1.1698	3.7104	0.9971
298.15	1.1044	3.4025	0.9925	0.9611	3.0500	0.9962
303.15	0.9644	2.9824	0.997	0.8075	2.5735	0.9922
308.15	0.8363	2.5736	0.9965	0.6172	1.9249	0.9999
313.15	0.7104	2.1662	0.999	0.4807	1.4611	0.9994

Table 2. Estimated interfacial energy values (mJ m^{-2}) using the 3D nucleation theory and the integral approaches for every saturation temperature (K).

	Integral Method				Classical 3D Approach (average)				Linearized Integral Method			
T_0	400 rpm		230 rpm		400 rpm		230 rpm		400 rpm		230 rpm	
	γ	$CV \times 10^{-2}$	γ	$CV \times 10^{-2}$	γ	R^2	γ	R^2	γ	R^2	γ	R^2
288.15	1.1	3.1533	1.3937	0.9967	1.2932	0.9964	1.363	0.9905	1.7896	0.9771	2.0315	0.9965
293.15	1.7387	5.5985	1.47	1.4672	1.4822	0.9971	1.4317	0.9909	2.1533	0.9838	2.1438	0.993
298.15	1.5149	2.2232	1.6227	0.9701	1.5902	0.9962	1.5345	0.9925	2.3065	0.9946	2.3289	0.9978
303.15	1.6	1.2353	1.672	1.9289	1.691	0.9922	1.6115	0.997	2.437	0.9996	2.4306	0.9971
308.15	1.8613	3.9726	1.795	1.6146	1.8716	0.9999	1.7012	0.9965	2.797	0.9725	2.5831	0.9988
313.15	2.2111	3.8422	1.9478	2.5227	2.0612	0.9994	1.8106	0.999	3.1822	0.9784	2.7798	0.9938

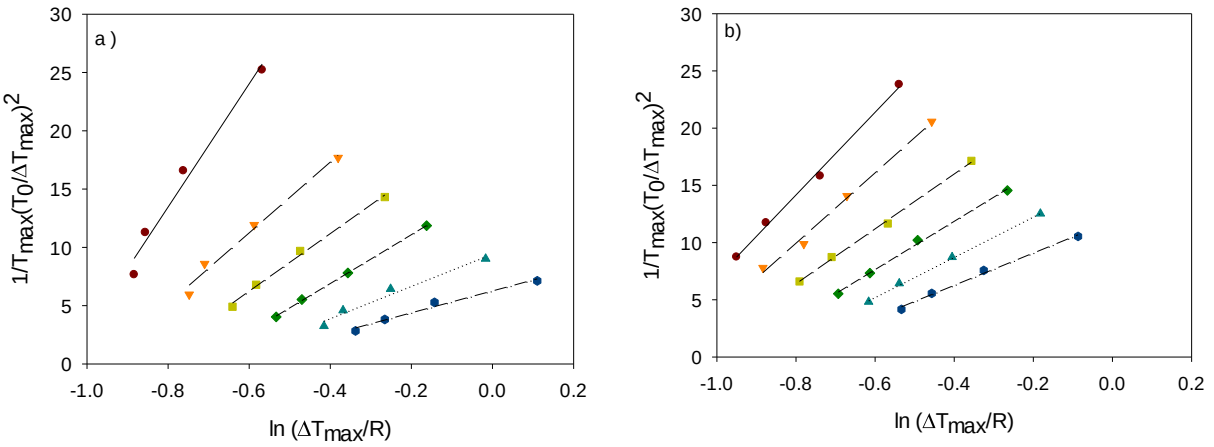

Figure 3. Experimental profiles (● 288.15 K, ▼ 293.15 K, ■ 298.15 K, ♦ 303.15 K, ▲ 308.15 K and ⬣ 313.15 K) vs calculated profiles (— 288.15, - - 293.15 K, - 298.15 K, – 303.15 K, ·· 308.15 K and – · – 313.15 K) using the linearized integral method at 400 rpm (a) and 230 rpm (b) respectively.

Conclusions

Regardless of the differences between the approaches used for estimating the interfacial energy, all three exhibited the same behavior with respect to the saturation temperature and the cooling rate. The differences between the integral method and the 3D nucleation theory are minimal, showing that the integral method is a good approximation for the calculation of interfacial energy. The interfacial energy increased when the saturation temperature increased. This behavior was in agreement with that shown by the MSZW. Larger interfacial energies hindered and delayed the birth of new nuclei; therefore, MSZW became wider.

Acknowledgments

The authors sincerely appreciate the financial support of the Consejo Nacional de Ciencia y Tecnologia (CONACyT) for the support of a PhD scholarship.

References

Chianese, A. and Kramer, M.J.H. (2012). *Industrial Crystallization Process Monitoring and Control*. Wiley-VCH, Weinheim.

Eder, R.J.P., Schrank, S., Besenhard, M.O., Roblegg, E., Woelfler, G.H. and Khinast, J.G. (2012). Continous sonocrystallization of acetylsalicylic acid (ASA): control of crystal size. *Crystal Growth and Design 12*, 4733-4738. https://doi.org/10.1021/cg201567y

Hansen, T.B., Taris, A., Rong, B., Grosso, M. and Qu, H. (2016). Polymorphic behavior of isonicotinamide in cooling crystallization from various solvents. *Journal of Crystal Growth 450*, 81-90. https://doi.org/10.1016/j.jcrysgro.2016.06.030.

Maia, G.D. and Giulietti, M. (2008). Solubility of Acetylsalicylic Acid in Etanol, Acetone, Propylene Glycol, and 2-Propanol. *Journal of Chemical Engineering Data 53*, 256-258. https://doi.org/10.1021/je7005693.

Medina, G.X.M. (2018). Medición del ancho de la zona metaestable de soluciones de ácido acetilsalicílico-etanol. Tesis de Maestría en Ciencias en Ingeniería Química, Instituto Tecnológico de Celaya, México.

Medina, G.X.M., Quintana, H.P.A., Reyes, V.J.N. and Fuentes, C.L.F. (2020). Determination of kinetic parameters of nucleation and growth for acetylsalicylic acid crystals in ethanol. *Revista Mexicana de Ingeniería Química 19*, 417-428. https://doi.org/10.24275/rmiq/Cat1574.

Medina, G.X.M., Quintana, H.P.A., Fuentes, C.L.F. and Martínez, G.G.M. (2022). Determination of primary nucleation kinetics of acetylsalicylic acid in ethanol. *Chemical Engineering &*

Technology 45, 1264-1270. https://doi.org/10.1002/ceat.202200109.

Mielniczek-Brzóska, E. (2014). Effect of sample volume on the metastable zone width of potassium nitrate aqueous solutions. *Journal of Crystal Growth 401*, 271-274. https://doi.org/10.1016/j.jcrysgro.2013.11.064.

Miyasaka, E., Kato, Y., Hagisawa, M., Hirasawa, I. (2006) Effect of ultrasonic irradiation on the number of acetylsalicylic acid crystals produced under the supersaturated condition and the ability of controlling the final crystal size via primary nucleation. *Journal of Crystal Growth 289*, 324-330. DOI: https://doi.org/10.1016/j.jcrysgro.2005.11.084.

Mohd, S.Z.N., Camacho, D.M., Yung, M.C. and Mahmud, T. (2020). Effect of crystallization conditions on the metastable zone width and nucleation kinetics of p-aminobenzoic acid in ethanol. *Chemical Engineering Technology 43*(6), 1105-1114. DOI: https://doi.org/10.1002/ceat.201900679.

Muñoz, A.A.O. (2020). Determinación del ancho de la zona metaestable de soluciones saturadas de nitrato de potasio en agua. Tesis de Maestría en Ciencias en Ingeniería Química, Instituto Tecnológico de Celaya, México.

Sangwal, K. (2009a). Novel approach to analyze metastable zone width determined by the polythermal method: physical interpretation of various parameters. *Crystal Growth Design 9*, 942-950. https://doi.org/10.1021/cg800704y.

Sangwal, K. (2009b). Novel self-consistent Nývlt-like equation for metastable zone width determined by the polythermal method. *Crystal Research and Technology 44*, 231-247. https://doi.org/10.1002/crat.200800501.

Sangwal, K. (2011). Some features of metastable zone width of various systems determined by polythermal method. *Crystal Engineering Communications 13*, 489-501. https://doi.org/10.1039/C0CE00065E.

Shiau, L.D. (2018). Determination of the nucleation and growth kinetics for aqueous L-glycine solutions from the turbidity induction time data. *Crystals 8*, 403. https://doi.org/10.3390/cryst8110403.

Shiau, L.D. (2020). A lineal regression model for determining the pre-exponential factor and interfacial energy based on the metastable zone width data. *Crystals 10*, 103. https://doi.org/10.3390/cryst10020103.

Shiau, L.D. and Wu, D.R. (2020). Effect of L-valine impurity on the nucleation parameters of aqueous L-glutamic acid solutions from metastable zone width data. *Journal Crystal Growth 546*, 125790. https://doi.org/10.1016/j.jcrysgro.2020.125790.

Shiau, L.D. (2021). A linearized integral model for determining the nucleation parameters from metastable zone width data. *Journal of Crystal Growth 564*, 126115. https://doi.org/10.1016/j.jcrysgro.2021.126115.

Sun, H., Gong, J.B. and Wang, J.K. (2005). Solubility of lovastatin in acetone, methanol, ethanol, ethyl acetate and butyl acetate between 283 K and 323 K. *Journal of Chemical & Engineering Data 50*, 1389-1391. https://doi.org/10.1021/je0500781.

Xiong, L., Zhou, L., Zhang, X., Zhang, M., Hou, B., Bao, Y., Du, W., Su, W., Zhang, S. and Yin, Q. (2018). Determination of metastable zone widths and nucleation behavior of aspirin in acetic acid and acetic anhydride binary solvent mixture. *Journal of Molecular Liquids 26*, 805-815. https://doi.org/10.1016/j.molliq.2018.08.055.

Zhang, X., Yang, Z., Chai, J., Xu, J., Zhang, L., Qian, G. and Zhou, X. (2015). Nucleation kinetics of lovastatin in different solvents from metastable zone width. *Chemical Engineering Science 133*, 62-69. https://doi.org/10.1016/j.ces.2015.01.042.